Electroless plating of buried contact solar cell

Dong Seop Kim, Eun Chel Cho and Soo Hong Lee

Photovoltaic Devices Lab, Materials & Devices Research Center, Samsung Advanced Institute of Technology, Suwon 440 - 600, Korea

전극함몰형 태양전지의 무전해도금

김동섭, 조은철, 이수홍

삼성종합기술원 태양전지팀, 수원, 440-600

Abstract The metallization is the key to determining cell costs, cell performance, and system reliability. Screen printing technology suffers from several limitations affecting mainly the front grid. The buried contact solar cell (BCSC) was specifically desinged to be compatible with low cost, mass production techniques and avoid the conventional metallization problem. By using electroless plating technique, we performed this metallization inexpensively and reliably. This paper presents the details of the optimization procedure of metallization schemes on laser grooved cell surfaces. Commercially available Ni, Cu and Ag plating solutions were applied for the cell metallization. The application of those solutions on the buried contact front metalliza-tion has resulted in an cell efficiency of 18.8 %. The cell parameters are an open circuit voltage of 651 mV, short circuit current density of 37.1 mA/cm^2, and fill factor of 77.8 %. The efficiency of over 18 % was achieved in the above 90 % of the batch.

요   약 태양전지의 전극형성은 전지의 가격과 성능 그리고 시스템의 신뢰성을 결정하는데 매우 중요한 변수이다. 기존의 스크린 프린팅 기술은 전면전극에 나쁜 영향을 미치는 여러가지 제약들을 가지고 있다. 전극함몰형 태양전지는 기존의 전극에서 발생하는 문제점을 극복하고 저가격 대량생산을 위해서 고안된 것이다. 본 논문에서는 무전해 도금방법을 사용하여 함몰형 전지의 전극을 형성하는 공정을 최적화함으로써 값싸고 재현성있게 전지를 제조할 수 있었다. 무전해 도금용액으로는 상업적으로 사용되는 니켈, 구리, 은 용액을 사용하였으며, 전지의 효율 을 최고 18.8 %까지 얻었다. 이때 전지의 개방전압은 651 mV, 단락전류밀도는 37.1 mA/cm^2,

충실도는 77.8 %였으며 배치에서 90 % 이상의 전지가 18 % 이상의 효율을 나타내었다.

1. Introduction

The concept of the buried contact solar cell (BCSC) evolved initially as a screen-printing approach for overcoming many fundamental limitations associated with conventional screen-printed metallization schemes. The most distinctive feature of the cell design is the use of grooves in the top surface to locate the cell metallization. Although originally investigated using screen printed metallization sequences, the most successful designs have used electrolessly plated metal contact [1-3]. In the case of printed contacts, expensive silver metal, poor metal aspect ratios, low conductivity of the screen-printed metals, the inability to produce fine lines and a relatively high contact resistance have placed severe limitations on the efficiencies achievable from conventional commercial approaches [4].

The key feature of the buried contact solar cell which differentiates it from the conventional screen printing technology is the front grid metallization. Unlike a screen printing technology, the buried contact front metallization reduces both low shading losses and series resistance losses because it has closely spaced, very fine metal lines and large cross sectional area of the metal in the grooves. In addition, the closely spaced metal fingers and low series resistance losses allow an lightly doped emitter, providing excellent response to short wavelength of light. Another feature of the buried contact solar cell which allow high efficiency operation is the heavy groove diffusion.

Following an economic evaluation of conductor layer metals for silicon solar cell metallization, base metal system utilizing copper, an inexpensive base metal, is a potential alternative to silver or solder. Copper, however, diffuses rapidly into silicon at low temperatures, degrading solar cell properties [5]. Nickel is shown to be a suitable barrier to copper diffusion as well as a desirable contact metal to silicon [6].

Metallization of buried contacts can be achieved by a variety of methods such as aluminium sputtering, evaporation, screen-printing and plating. The significant benefits of plated contacts are low cost process, reduced material usage (metal is deposited only where required), their suitability to textured surface and independence of contact shape (metal is easily deposited in the groove). Interest in electroless plating has continued unabated since its invention by Brenner and Riddell in 1946 [7].

In this work, the metallization was carried out by plating metal on the oxide free surfaces within the grooves by electroless chemical deposition. We discussed on the problem of metallization of BCSC cells and its solution in detail. The metals used for contact formation were nickel, copper and silver [8].

2. Experimental

Float zone wafers of 0.5 Ω·cm resistivity and 500 μm thickness were used as substrates. To minimize reflection losses, the top surfaces of wafes were chemically textured in 2 % NaOH solution. Emitter diffusion was carried out on the diffusion furnace by using phosphorus pentoxide solid source. For antireflection control, masking the second diffusion and high quality surface passivation as well as good metal contact passivation, the textured surface was oxidized. The metal grid was defined by scribing deep grooves through the masking oxide. The scribing was done by using laser scriber. After chemical etching of the grooves to remove residues, a second phosphorus diffusion was carried out more heavily than before. Phosphorus was diffused in the grooves to dope the silicon beneath the metal contact. Aluminium was deposited onto rear of the cell by electron beam evaporation and sintered to form an ohmic contact and back surface field. The wafers were immersed in the buffered HF acid bath to remove all the oxide from the grooves (deglazing step). The buffered etching solution consists of hydroflouric aicd (49 % HF) and ammonium flouride (40 % NH₄F). To deposit a thin layer of nickel on the bare silicon surface in the grooves and on the rear surface we used ammonia based nickel plating solution. The pH of the solution was above 8.5 and the temperature was 85 ∼ 90 ℃. After nickel plating wafers were sintered at 300 ∼ 400 ℃ in a non-oxidizing ambient to form a good

electrical and mechanical contact between the silicon and the nickel. Nickel oxidizes very easily producing an oxide which is both mechanically and chemically very resistant. Therefore, we designed nickel sintering furnace to avoid oxidation of nickel during sintering. The diagram of sintering furnace is given in Fig. 1. The wafers were immersed in Cu plating solution to fill the grooves with copper so as to provide adequate current carrying capacity while minimizing the shading loss on the top surface of the cell. The composition of the plating solution should be controlled to fill the groove completely. Silver was plated to form a protective coating on the copper so as to prevent oxidation of the copper and to provide a readily solderable surface without the use of corrosive soldering flux. Efficiencies are measured relative to reference cells. The reference cells used are calibrated by Sandia National Laboratory, U.S.A and University of New South Wales, Australia. Manufacturing process above discribed is given in Fig. 2. Figure 3 shows schematic diagram of a buried contact solar cell fabricated on single crystalline silicon.
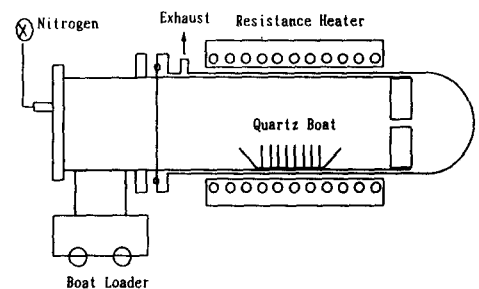

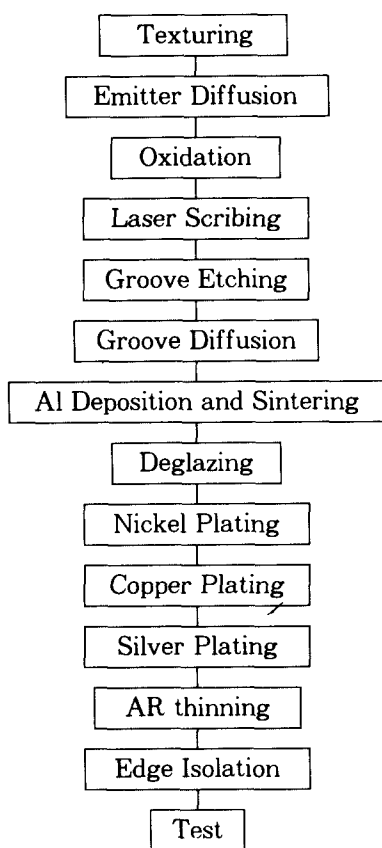Fig. 1. Schematic diagram of the nickel sintering furnace.
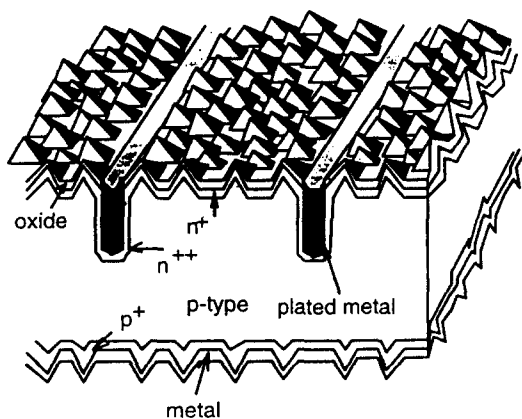
Fig. 2. The process sequence for BCSC.

Fig. 3. Schematic diagram of a buried contact solar cell fabricated on single crystalline silicon.

3. Result and discussion

The oxide forms in the grooves during the phosphorus groove diffusion. In order to know the effects of the oxide in the groove on the metallization process, we deglazed grooves for $10 \sim 50$ seconds and then plated nickel, copper and silver in the grooves. The buffered etching solution consists of hydroflouric acid (49 % HF) and ammonium flouride (40 % NH$_4$F). Figure 4 shows deglazing times and their effects on the cell parameters.

As the deglasing time increased from 10 sec to 40 sec, all the parameters increased and then decreased with further increasing deglazing time. The short circuit current density and open circuit voltage are given by
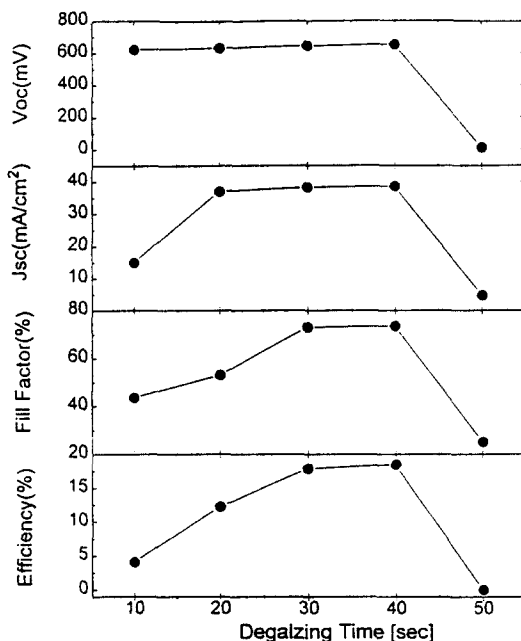

Fig. 4. Cell parameters of BCSC as a function of the deglazing time.

$$J_{SC} = \left[1 + \frac{R_S}{R_{Sh}} \right]^{-1} \left[J_0 \left\{ \exp\left(\frac{qJ_{SC}R_S}{AkT} \right) - 1 \right\} - J_L \right]$$

$$(1)$$

$$V_{OC} = \left(\frac{AkT}{q} \right) \ln\left[\frac{J_L - \left(\frac{V_{OC}}{R_{Sh}} \right)}{J_0} + 1 \right] \qquad (2)$$

where J_0 is the reverse saturation current density, R_s is series resistance R_{sh} is shunt resistance, q is electronic charge, J_{sc} is short circuit current density, A is diode ideality factor, k is Boltzmann's constant, J_L is photogenerated current density. It is seen that V_{oc} is unchanged by simple R_s and that J_{sc} is changed very little unless R_s is quite large. The fill factor is determined by the magnitude of the V_{oc}, A, R_s and R_{sh} and seriously reduced as R_s increased. It seems, therefore, that the changes of parameters in Fig. 4 are mainly caused by series resistance. Electroless nickel plating on silicon is based on a catalytic oxidation-reduction reaction between nickel ion (Ni^{2+}) and hypophosphite ($H_2PO_2^-$) ion at the catalytic (conductive) surfaces with input of external energy. The
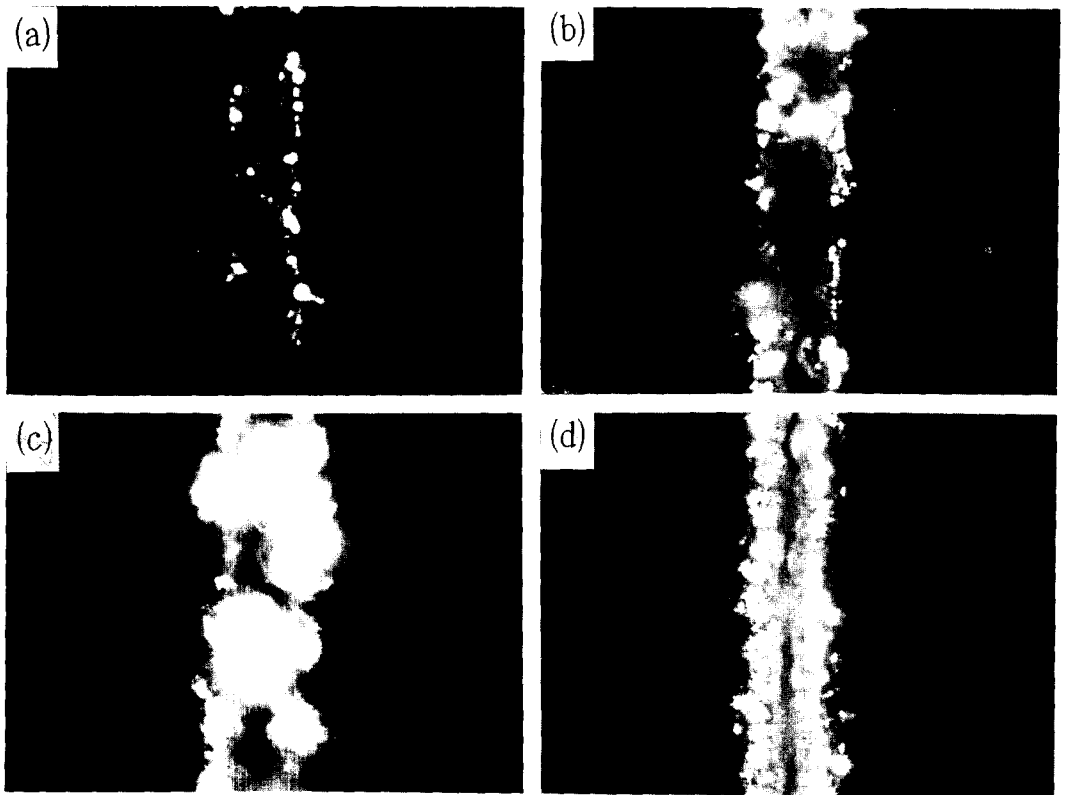

Fig. 5. Optical microscope photographs of grooves after copper plating (5 hrs) and silver plating (2 min). Deglazing time was 10 sec for (a), 20 sec for (b), 30 sec for (c) and 40 sec for (d).

hypophosphite anions in aqueous medium is oxidized to the phosphite ion with evolution of H, the rate being a function of temperature and hypophosphite concentration [9]. On the basis of organic analogies, nickel plating is assumed to be a catalytic dehydrogenation of the hypophosphite molecule according to the equation :

$$2H_2PO_2^- + Ni^{2+} + 2H_2O$$
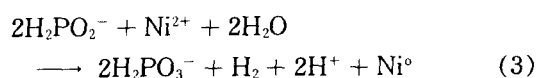$$\longrightarrow 2H_2PO_3^- + H_2 + 2H^+ + Ni^\circ \qquad (3)$$

Figure 5 shows surfaces of grooves after copper plating. If the grooves are not completely cleared of oxide then the subsequent nickel plating will not work well and the grid line is not continuous because nickel will not plate on an insulating oxide. The discontinuous grid line cause the series resistance of cell high. The efficiency increases as the deglazing time increases due to the reduction of series resistance. Nickel was plated not only in the groove but also on the top of pyramid when deglazing time is longer than 50 sec. Figure 6 shows the nickel spot plated on the top of the pyramid. The textured front surface may lead to non-uniformity in etching the oxide on the front surface. The oxide-coated top of pyramid is exposed to heavy phosphorus diffusion during groove diffusion. Phosphorous doped oxide etches more quickly and the peaks of the pyramids are more exposed to the etching solution. If the oxide is removed from these pyramid peaks, nickel is plated easily on them. During the subsequent copper plating all over the surface was covered with copper because copper is easily plated on the nickel on the top of the pyramid. Therefore, cell parameters drops quickly when oxide on the top of the pyramid is removed as shown in Fig. 4. The copper plating solution used is
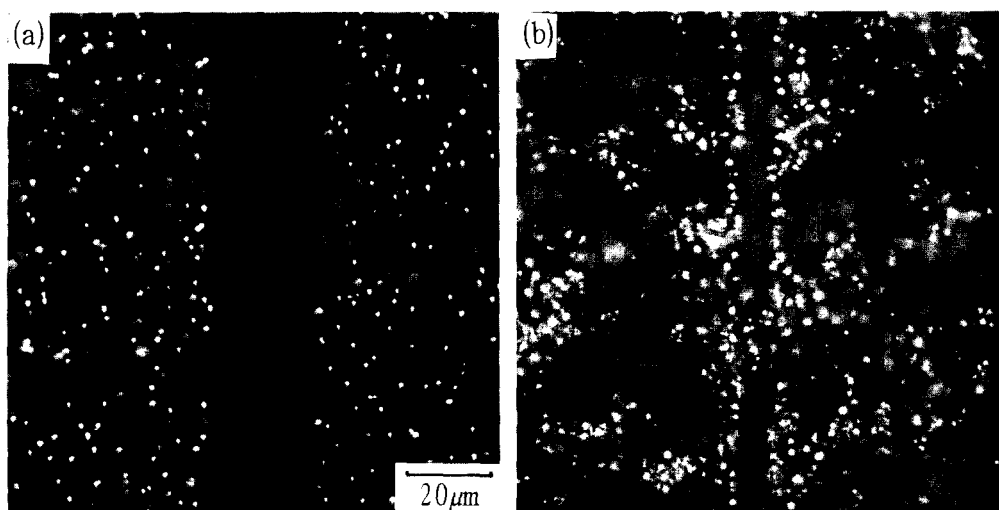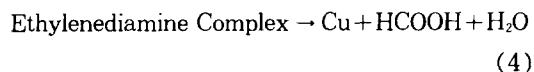

Fig. 6. Optical microscope photographs of front surfaces after nickel plating (a) and after copper plating (b). Deglazing time was 50 sec.

Enplate Cu-704 supplied by Ethone OMI. The plating process is based on a catalytic surface reaction between the formaldehyde and cupric ions (Cu^{2+}).

$$Cu^{2+} + HCHO + 2OH^- \rightarrow$$

Ethylenediamine Complex $\rightarrow Cu + HCOOH + H_2O$

$$(4)$$

Ethylemediamine derivative, which is a vital catalyst, combines with the cupric ions to form an square complex ion in solution. The geometry of chelator copper complex facilitates the transfer of an electron from any conductive surface to the cupric ion creating a bond between the surface and the Cu atom, and thus initiating the plating process.

Figure 7 shows optical microscope photographs of the top of the copper plated groove with plating time. Copper started to plate from the wall of the groove filling the groove. The copper finger width increased as plating takes place at the mouth of the
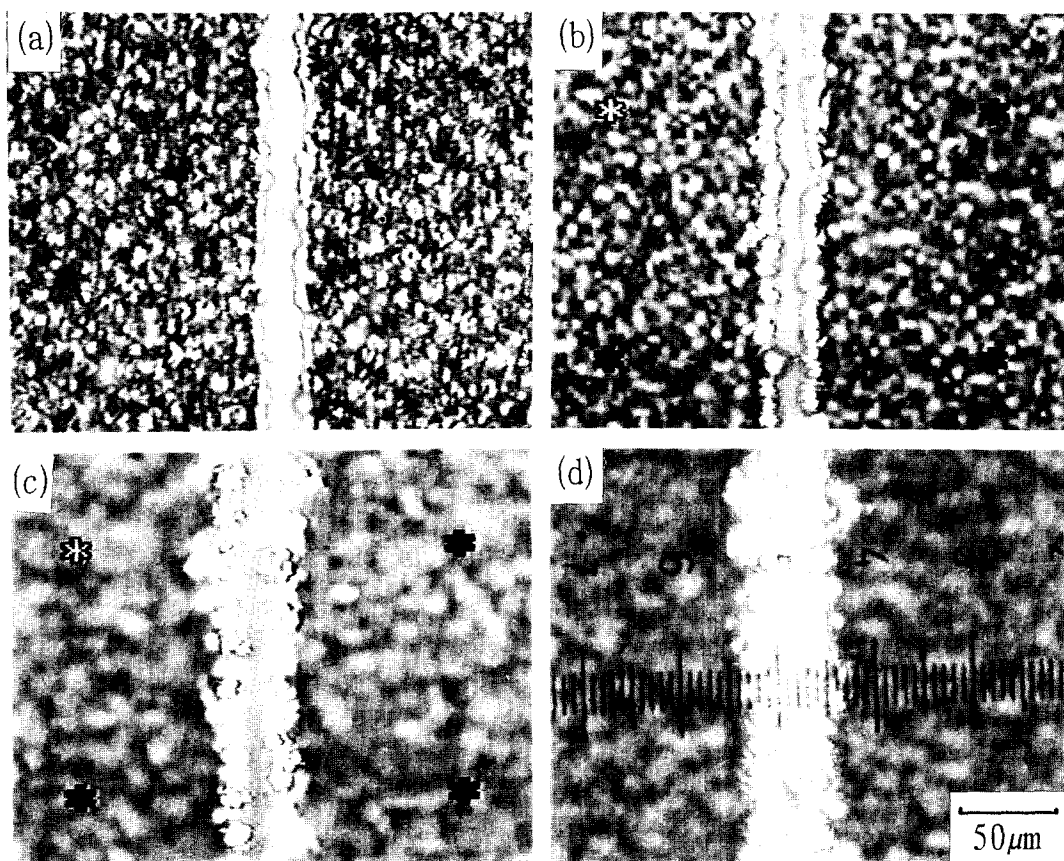

Fig. 7. Optical microscope photographs (×500) of the top of the groove during copper plating. Copper plating time was 2 hr for (a), 3 hr for (b), 4 hr for (c) and 5 hr for (d).
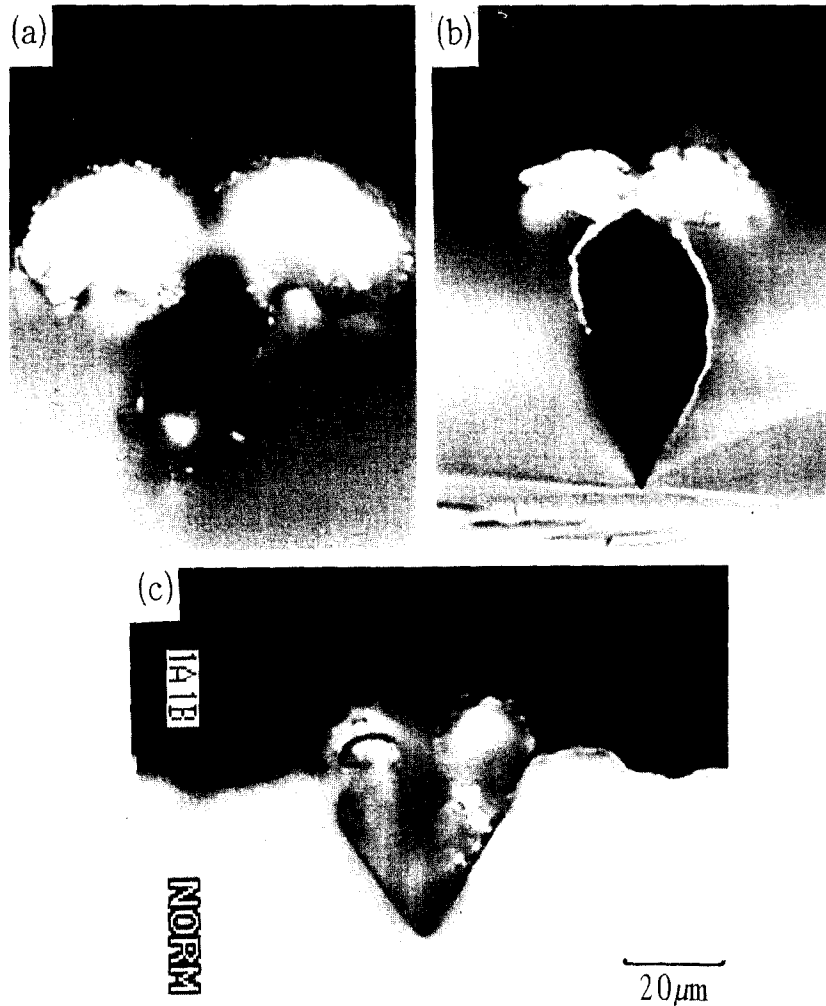
Fig. 8. Optical microscope photographs of crossection of the grooves. Cupric ion concentration was 10g/L : (a), 6g/L : (b), (c).

groove and spreads across the surface with increasing plating time. Optical micrographs of cross-section of partially filled grooves (a,b) and a fully plated groove (c) are given in Fig. 8 for comparison. The main constituents affecting copper plating rate in our plating solution were the concentration of cupric ion (Cu^{2+}), NaOH and HCHO. Cu-pric ion concentration was changed to control the plating rate with the concentrations of NaOH and HCHO fixed. If the copper plating rate is too high (a) or the groove is too deep (b) the mouth of the groove becomes blocked with copper before filling the groove compeletely. The composition of the plating should be regularly monitored by
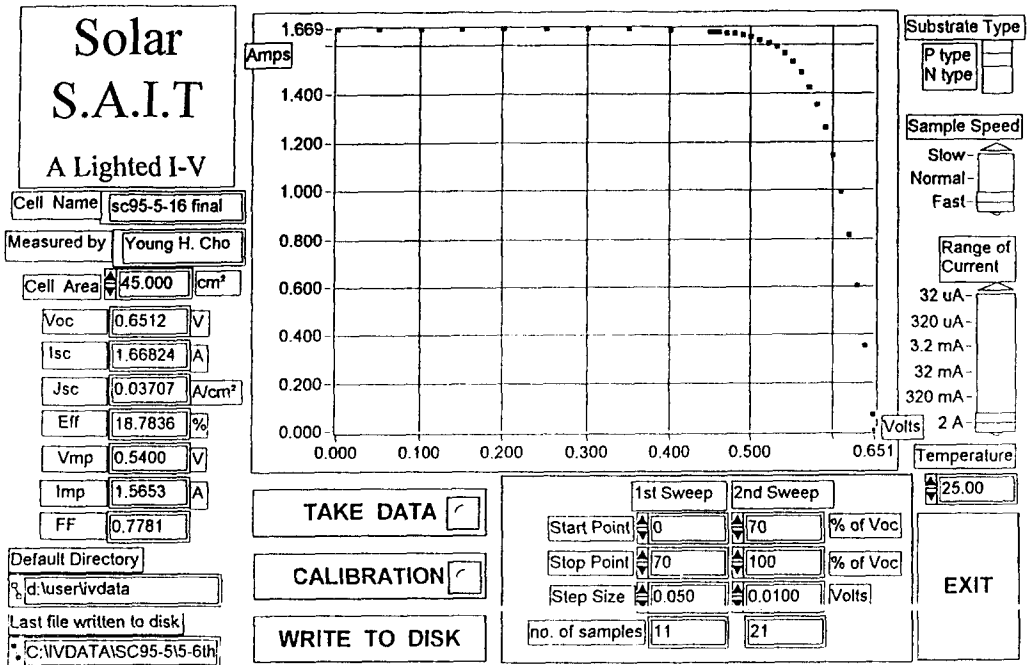
Fig. 9. Current-Voltage curve of BCSC fabricated at SAIT.

chemical analysis and replenished whenever it is necessary. We noted that the width of copper fingers should be no more than 60 μ m to reduce shading loss.

Current-voltage curve of BCSC fabricated at SAIT (Samsung Advanced Institute of Technology) is shown in Fig. 9. The highest efficiency is 18.8 % and its cell parameters are an open circuit voltage of 651 mV, short circuit current density of 37.1 mA/cm², and fill factor of 77.8 %. The efficiency of over 18 % has been obtained in the above 90 % of the batch.

4. Conclusion

For the metallization of BCSC, commer-

cially available Cu, Ni and Ag electroless plating solutions were applied. Nickel dose not plate on an insulating oxide and the grooves must be thoroughly deglazed. Nickel was plated, however, on the top of the pyramid when the deglazing time is too long. Care must be taken to ensure that the thickness of the masking oxide at the peak of the pyramids after deglazing is adequate to effectively mask against copper plating. If the copper plating rate is too high or the groove is too deep the mouth of the groove becomes blocked with copper before filling the groove compeletely with copper. This will drop fill factor or the current density of the solar cell. By appropriate blending of the four constituent components we can control the plating characteristics such as plating

speed and plating quality. The application of those solutions on the buried contact front metallization has resulted in a cell efficiency of 18.8 %. The cell parameters are an open circuit voltage of 651 mV, short circuit current density of 37.1 mA/cm^2, and fill factor of 77.8 %.

References

[1] L.A. Grenon, N.G. Sakiotis and M.G. Coleman, Reliability of Silicon Solar Cells with a Plated Nickel-Copper Metallization System, Conf. Record, 15th IEEE PVSC (1981) p. 522.

[2] D.P. Tanner, P.A. Iles and P. Alexander, An All-Plated, Low Cost Contact System for Silicon Solar Cells (1980) p. 800.

[3] S.R. Wenham, Buried Contact Silicon Solar Cells, Progress in photovoltaics, Vol. 1 (1993) pp. 3-10.

[4] M.A. Green, green, Silicon Solar Cells Advanced Principles & Practice, Printed by Bridge Printery Pty. Ltd., p. 236.

[5] M.G. Coleman, R.A. Pryor and T.G. Sparks, A Base Metal System for Silicon Solar Cells, Conf. Record 14th IEEE PVSC (1980) p. 793.

[6] D.P. Tanner, P.A. Iles and P. Alexander, Conf. Record, 14th IEEE PVSC, Las Vegas (1991).

[7] A. Brenner and G.E. Riddell, J. Res. Nat'l. Bur. Stan. 37, 31 (1946) ; Proc. Am. Electroplat. Soc. 33, 23 (1946).

[8] S.R. Wenham, Laser Grooved Silicon Solar Cell, Ph. D. Thesis (1986), University of New South Wales.

[9] A.W. Goldenstein, et al., J. Electrochem. Vol. 104(2) (1957) 104.